Significance of Conceptual Model Uncertainty in Simulating Carbon Sequestration in a Deep Inclined Saline Aquifer

Ye Zhang[1]; Guang Yang[2]; and Shuiquan Li[3]

Abstract: In modeling geologic carbon sequestration in a deep inclined aquifer in Wyoming, the impact of geologic, engineering, and environmental uncertainty factors on parameter importance and prediction uncertainty is evaluated. Given site characterization data, a suite of geologic model families were built to represent aquifer permeability heterogeneity at increasing complexity. With each family, the same CO_2 experiment was simulated. Over a period of 50 years, 17 million tons of CO_2 is injected into the aquifer at an approximate depth of 3,750 m. Postinjection simulation is then carried out for a total simulation time of 2,000 years. Based on the design of the experiment, a screening sensitivity analysis was first conducted for all families, systematically varying uncertain input parameters. Parameters with first-order impact on CO_2 performance metrics (i.e., trapped gas, dissolved gas, brine leakage, storage ratio) are identified, which vary with time and modeling choice. When the model is of low complexity, engineering and environmental factors are identified as the most significant; when the model increases in complexity, geologic factors that influence aquifer heterogeneity become more important. Given the screening test outcome, a response surface analysis was carried out for each family to create prediction envelopes of the CO_2 storage ratio. By the end of injection, all families predicted similar uncertainty in the storage ratio. After injection ceases, prediction envelopes of the families deviated gradually from one another as a result of different large-scale heterogeneity experienced by each family because the plume migrated continuously along dip. For this inclined aquifer, resources should be devoted first to characterize geologic uncertainty factors (i.e., porosity-permeability transform and facies correlation structure) that influence permeability magnitude and connectivity. The effect of these factors on CO_2 flow, trapping, and storage becomes overwhelmingly important compared with engineering and environmental factors. Under conditions of low formation temperatures and high formation fluid pressures, representative CO_2 plumes corresponding to end member CO_2 storage ratios become gravity-stable. **DOI: 10.1061/(ASCE)HZ.2153-5515.0000246.**

Author keywords: Carbon storage; Deep saline aquifer; Geologic modeling; Uncertainty; Gravity-stable flow.

Introduction

Geological carbon sequestration (GCS) is considered a promising option to reduce the atmospheric loading of carbon dioxide [Intergovenmental Panel on Climate Change (IPCC) 2005]. Wyoming produces approximately 40% of the nation's coal, and in 2000 its coal-fired power plants emitted approximately 51 million tons (Mt) of CO_2 into the atmosphere. By 2009, the emission rate has risen to 54.4 Mt/year and it is projected to increase with new energy demand (Deng et al. 2012). To sequester CO_2 at industrial scales, deep saline aquifers with large storage capacity are needed (Bachu 2003). As part of a larger study, this paper investigates the Nugget Sandstone in western Wyoming (Fig. 1), which lies close to several power plants. Extending from the near surface towards a depth of ~20,000 ft, it is a regional deep saline aquifer with an average thickness of 600 ft and an average dip angle of ~16° (east-west). The site lies northeast of several oil fields with hydrocarbon production from the same formation (Fig. 1), while multiple caprocks, including the extensive Hilliard shale, provide a seal for the reservoirs (Royse 1993; Harstad et al. 1996). Due to hydrocarbon production and recent interest in GCS, a variety of subsurface static characterization data exist for this formation, e.g., wireline logs, core measurements, and seismic data (Frost 2011; Li et al. 2011b). To predict CO_2 storage, a geologic model describing spatial variation of aquifer properties such as porosity (ϕ) and intrinsic permeability (k) can thus be created, which provides input to a fluid flow simulator. This study conducts an uncertainty analysis to understand the importance of various uncertainty sources on predicting key GCS performance metrics, e.g., residually trapped and dissolved CO_2, brine leakage, and CO_2 storage ratio. Both CO_2 flow during injection and its long-term migration are of interest because inclined aquifers can lead to different trapping behaviors from that observed in aquifers without significant dips (Ide et al. 2007; Hesse et al. 2008; Macminn et al. 2010).

In modeling GCS, uncertainty sources include static or geologic factors that influence aquifer heterogeneity, and engineering and environmental factors that influence CO_2 trapping and migration. In a scoping study, factors identified to exert the largest impact on storage (or other prediction metrics) are the focus for characterization. Compared with earlier works addressing parameter uncertainty (Sifuentes et al. 2009; Beni et al. 2011; Liu et al. 2011; Bandilla et al. 2012), this study emphasizes the uncertainty in developing a conceptual site model, which is believed to be high because most deep saline aquifers are data poor. As a result,

[1]Associate Professor, Dept. of Geology and Geophysics, Univ. of Wyoming, 1000 University Ave., Laramie, WY 82071 (corresponding author). E-mail: yzhang9@uwyo.edu

[2]Dept. of Energy Resources Engineering, Stanford Univ., 367 Panama St., Green Earth Sciences 065, Stanford, CA 94305.

[3]Enhanced Oil Recovery Institute, Univ. of Wyoming, Laramie, WY 82071.

Note. This manuscript was submitted on February 21, 2014; approved on August 11, 2014; published online on September 17, 2014. Discussion period open until February 17, 2015; separate discussions must be submitted for individual papers. This paper is part of the ***Journal of Hazardous, Toxic, and Radioactive Waste***, © ASCE, ISSN 2153-5493/04014036(14)/$25.00.

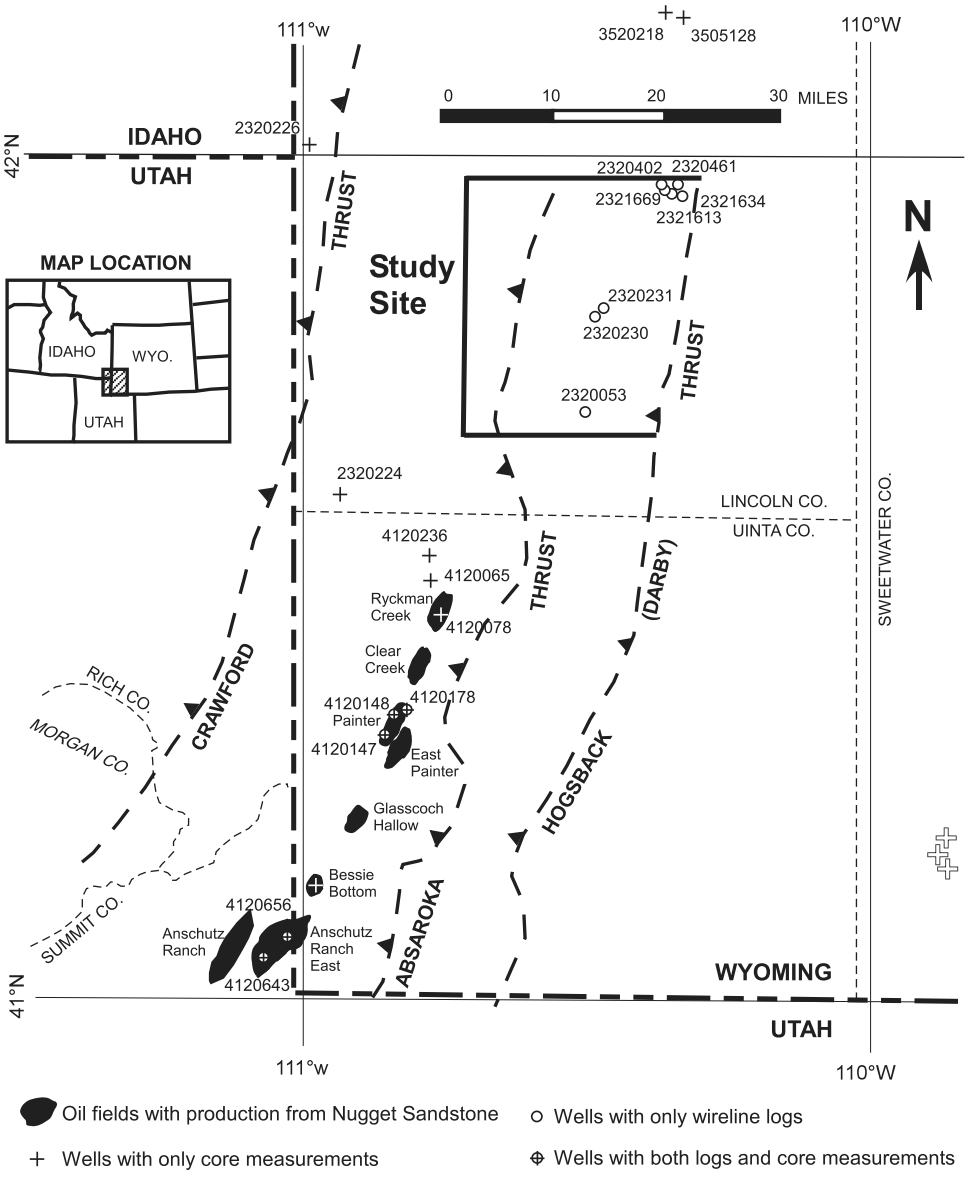

Fig. 1. Study site showing the location of wells that perforate the Nugget Sandstone [American Petroleum Institute (API) number is indicated at each well location]; hollow crosses indicate core location from the stratigraphically equivalent Weber Sandstone Fox et al. (1975); some data used in this paper are located outside the map area

depending on the type, amount, and accessibility of data, geologic models of different complexity can be built, where aquifer permeability is assumed homogeneous or heterogeneous (Stauffer et al. 2009; Han and McPherson 2009; Lu et al. 2009; Li et al. 2011a; Bandilla et al. 2012; Deng et al. 2012). Will such conceptual uncertainty, which varies with data support and the modeler's experience, skills, and perception of site geology, affect the uncertainty outcomes? In other words, when a site model is conceptualized at a different complexity, will this change the key uncertainty factors and associated prediction uncertainty? To test this idea, this study built a suite of increasingly complex geologic model families for the Nugget Sandstone using increasing amount of static site characterization data. For each model family, geologic, engineering, and environmental uncertainty factors are evaluated to identify those that significantly impact CO_2 predictions. This paper follows Li and Zhang (2014), which evaluated the same formation in a neighboring region where the sandstone exhibits a weak incline with an average formation dip <3° (Royse 1993). At that site, conceptual uncertainty did not significantly impact CO_2 predictions. However, because dipping aquifers can contribute to enhanced dissolution (Ide et al. 2007; Kumar et al. 2004) while affecting the shape and speed of plume migration (Mosthaf 2007), the previous result may not be applicable here.

Besides conceptual uncertainty in creating a site model, storage security, i.e., leakage risk of the injected CO_2 back to the surface, is an important concern. At the typical depths considered for GCS (1–3 km), CO_2 is a supercritical fluid (referred to herein as gas) with a lower density than that of formation brine. Its migration is driven by buoyancy, where the injected gas rises up and flows toward the caprock. However, in industrial storage where the CO_2 footprint can be significant, finding perfect caprock at large scales is problematic because a variety of leakage pathways exist in caprocks, e.g., faults and fractures (Konstantinovskaya et al. 2014), lateral facies changes (Fleury et al. 2010), and leaky wellbores (Nordbotten et al. 2005). To reduce the leakage risk, deeper injection (where CO_2 is gravity-stable) provides an attractive alternative.

When injection horizon is deep, CO_2 under high pressure can have a density exceeding that of the brine (Firoozabadi and Cheng 2010) and the injected gas may sink to the aquifer bottom instead of rising upwards. Deeper injection also gives rise to a higher storage capacity because more CO_2 mass can be stored per unit pore volume (Bachu 2003). To date, deeper injection has not been investigated extensively in GCS field and simulation studies (Michael et al. 2010), although limited evidence suggests its viability. For example, in western Wyoming, acid gas disposal into the Madison Limestone has been ongoing since 2005 without reporting leakage. The injection depth is at 5,334 m (Huang et al. 2011), greatly exceeding the depths considered for GCS. At that site, when CO_2 injection into the Nugget Sandstone was simulated at a depth of 4,200 m (Li and Zhang 2014), gravity-stable flow was observed. Whether such condition can develop in the same (although inclined) formation and the associated storage security are of interest. Besides depth, other factors can also influence CO_2 density, e.g., increasing reservoir temperature may reduce density, offsetting the effect of increased depth (pressure). Near the injector, low-permeability facies can create flow barriers, regardless of the migration direction. All these factors are uncertain at the study site.

Using a computationally efficient uncertainty analysis, this study evaluates both the impact of model complexity on CO_2 predictions and the competing processes and effects that can contribute to CO_2 migration and leakage. The uncertainty analysis is based on the design of experiment (DoE) and response surface (RS) method, which can be used to efficiently explore parameter and prediction space in a simulation study (Yeten et al. 2005; Montgomery 2008). Subsequently, a study overview is presented, followed by a list of uncertainty sources identified at the study site and the analysis method. For four model families with increased complexity, parameter sensitivity and prediction uncertainty are compared. Plume footprints are analyzed to evaluate conditions for gravity-stable flow. Insights obtained are discussed and summarized.

Uncertainty Analysis

Overview

For the Nugget Sandstone at the study site, four families of geologic models are built representing alternative conceptual models created with increasing data. For each family, key geologic and engineering and environmental uncertainty factors are identified, followed by an RS analysis to assess prediction uncertainty in modeling the CO_2 storage. Results are compared among the families, yielding insights into the effect of model complexity on parameter importance and prediction uncertainty. Because CO_2 flow can be dominated by viscous force during injection and gravity force after injection ceases, important factors influencing an outcome can change with time. Results of the uncertainty analysis are evaluated over multiple time scales. This study consists of three main steps:

1. Four model families with increasing complexity are created, which range from a deterministic homogeneous model to a hierarchical stochastic model conditioned to hard and soft data.
2. For each family, a screening sensitivity analysis (SA) is carried out to identify key input factors that impact selected CO_2 prediction outcomes. These parameters are considered important factors that need to be better characterized. For a given outcome, parameter importance is compared among the families and over time.
3. For each family, based on the key factors identified previously, an RS analysis is conducted to assess uncertainty in predicting CO_2 storage. This step consists of (1) generating an RS design with the key factors, (2) verifying an RS model within the parameter bounds of the RS design, and (3) creating prediction envelopes of CO_2 storage using Monte Carlo sampling with the RS model. The storage uncertainty is also compared among the families and over time.

In Step 2, the outcomes of interest are (1) brine leakage from model's open boundaries, (2) residual gas saturation (i.e., supercritical CO_2 trapped in pore space due to capillarity), (3) dissolved CO_2 molar fraction in brine, and (4) storage ratio $(\mathrm{SR}) = (\text{mass of dissolved } CO_2 + \text{mass of residual } CO_2)/(\text{mass of injected } CO_2)$. Compared with residual and dissolved CO_2, the remaining supercritical CO_2 (i.e., mobile gas) continues to migrate under buoyancy, posing a leakage risk. Each outcome is examined at multiple simulation output times, including end of injection and end of simulation.

In the uncertainty analysis, input parameters can be fixed (those that typically vary little at a storage site) or variable (the so-called factors). The latter group includes geologic factors (GFs) and engineering and environmental factors (EEFs). Geologic factors are those whose variations control aquifer permeability distribution and are thus related to static model uncertainty. EEFs include reservoir dynamic properties and environmental condition such as relative permeability model (RPM), residual gas saturation (RGS), temperature gradient (TG), vertical to lateral permeability (VHR) (k_V/k_H), and brine salinity (SAL). These factors and their uncertainties are considered independent of aquifer heterogeneity and the geologic factors contributing to it, and are thus included in the uncertainty analysis for each model family. In the following, sources of each uncertainty and their variations are presented.

Sources of Uncertainty: Engineering and Environmental

CO_2 storage can be affected by residual trapping due to gas-phase relative permeability hysteresis (Li et al. 2011a, b; Liu and Zhang 2011). Because relative permeability is not available for the Nugget Sandstone, laboratory measurements on different sandstone cores were used (Bennion and Bachu 2006b; Benson 2006). Capillary pressure, measured on the same cores, was also obtained. In the uncertainty analysis, two RPMs are chosen based on their end points: +1 (Cardium Sandstone); −1 (Berea Sandstone) (Fig. 2). In the Cardium Sandstone, due to its high endpoint relative permeability, CO_2 can flow at nearly three times the speed of the Berea Sandstone. Because postinjection storage is often dominated by imbibition, i.e., water invading pores initially filled with CO_2, for a given RPM, magnitude of residual gas saturation (which controls the amount of capillary trapping) is also varied. RGS is assumed independent of RPM because CO_2-brine relative permeability can vary with temperature, pressure, and pore-scale characteristics (Bennion and Bachu 2006a) and suffers considerable uncertainty for an aquifer with large variations in these characteristics.

End member temperature gradients are inferred from available temperature logs in study area (Fig. 3). Given the depth range of interest (~2,100 m above sea level to 3,600 m below sea level), these gradients generate either a cool (−1 end member) or a warm (+1 end member) model, which affects CO_2 density, gravity segregation, and migration. To determine the range of k_V/k_H, core measurements from the Nugget Sandstone and its equivalent formations are collected (Fig. 1 shows a subset of core locations). From these measurements, significant variation of k_V/k_H is observed (Fig. 4). Because both open and sealed fractures can occur in sandstones (Lindquist 1983; Laubach et al. 2010), end member k_V/k_H are fitted: 2.0 (+1) and 0.02 (−1). In a geologic sense, the

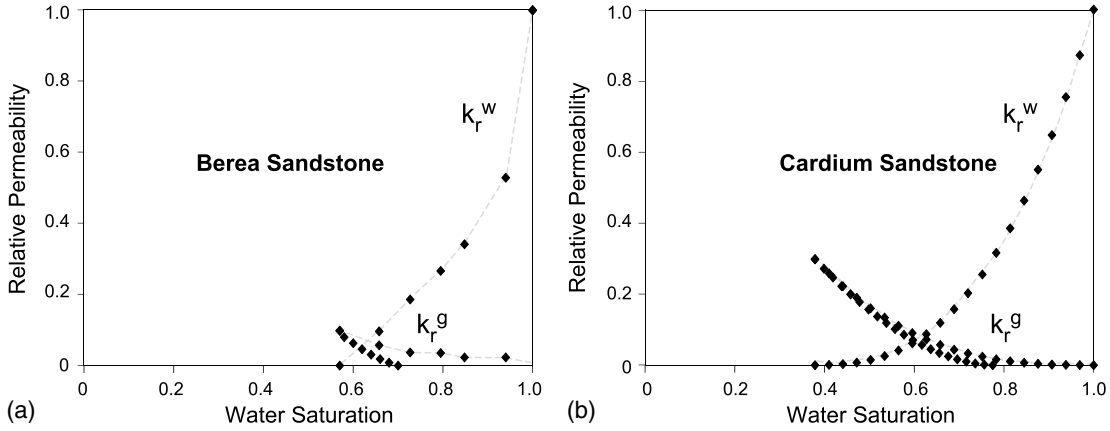

Fig. 2. Relative permeability end members; k_r^g and k_r^w are relative permeability of supercritical CO_2 and brine, respectively; imbibition curve of the Berea Sandstone is modified to allow residual trapping under the +1 end member of RGS: (a) Berea Sandstone; (b) Cardium Sandstone

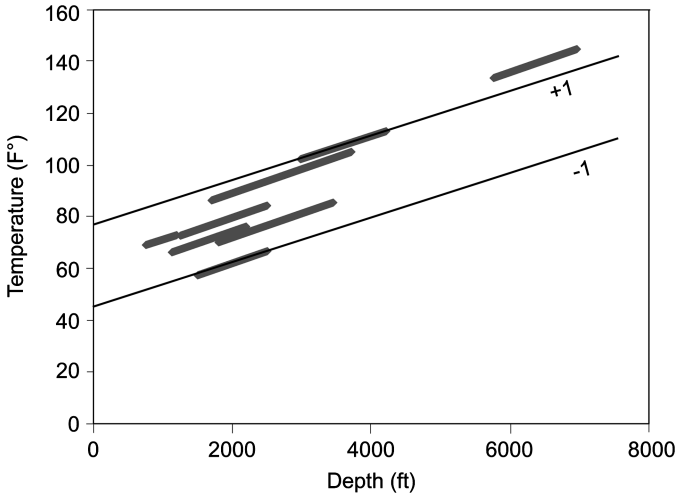

Fig. 3. Temperature-depth measurements from well logs at and near the study site, obtained from relatively shallow depths; end member TG are inferred from the measurements

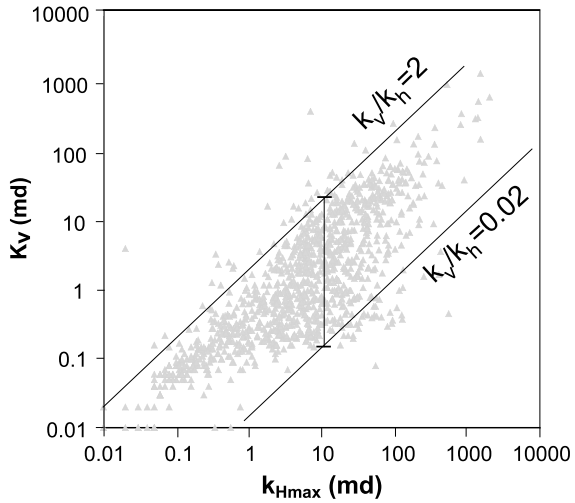

Fig. 4. Vertical and horizontal permeability measurements from Nugget Sandstone cores; end member VHR (k_v/k_H) are fitted to the data

+1 case can represent high-angle open fractures, while the −1 case can correspond to matrix anisotropy, cores with sealed fractures, or other mechanisms (Lewis and Couples 1993; Laubach 2003; Morad et al. 2010). Finally, SAL is varied based on observed salinities of Nugget formation brines in study area (Li et al. 2011b). Higher salinity results in less CO_2 dissolution.

Sources of Uncertainty: Geologic Modeling

To build the geologic models, a variety of field and laboratory characterization data are collected, screened for accuracy, and analyzed, including wireline logs, core porosity and permeability, cross sections, and isopach maps. Using subsets of these data, a suite of increasingly complex model families are built: homogeneous model (FAM1), stationary geostatistical facies (FAM2a) and petrophysical (FAM2b) models, stationary facies with subfacies petrophysical variability (FAM3), and nonstationary facies (with subfacies variability) conditioned to hard and soft data (FAM4). The model building procedure, including an upscaling step to convert data at well-log resolutions to simulation grid cells, is described in Li et al. (2011b) and Yang (2012), thus only an overview is presented here.

In building the models, the first step is to create a structure model conditioned to well logs (i.e., FAM1). For example, surfaces such as Nugget top and Nugget bottom were created from correlating well logs containing information about formation contacts. Within the structure model, facies (i.e., FAM2a) or petrophysical properties (i.e., FAM2b) can be populated using geostatistical techniques, which ensure that model properties are conditioned to relevant well data. After a facies model is created, petrophysical properties can be assumed homogeneous within each facies (i.e., FAM2a) or heterogeneous (i.e., FAM3). And if geologic insights exist suggesting the existence of a trend (e.g., certain facies becomes replaced by another facies), the previous model, which distributes the facies in equal probability spatially, can be conditioned to soft data such as a facies probability cube, which describes such a trend (i.e., FAM4). The model families were built with *Petrel 2009* (Schlumberger 2009b), and all models were checked for consistency against data.

To facilitate model comparison, the families share the same external geometry ($L_x \simeq 7{,}004$ m, $L_y \simeq 9{,}023$ m, $L_z \simeq 183$ m; x extends east-west and y extends north-south), simulation grid ($N_x = 126$, $N_y = 162$, $N_z = 15$, for a total of 306,180 cells), CO_2 injection design (e.g., well location, injection rate and duration, bottomhole pressure constraints), and boundary conditions.

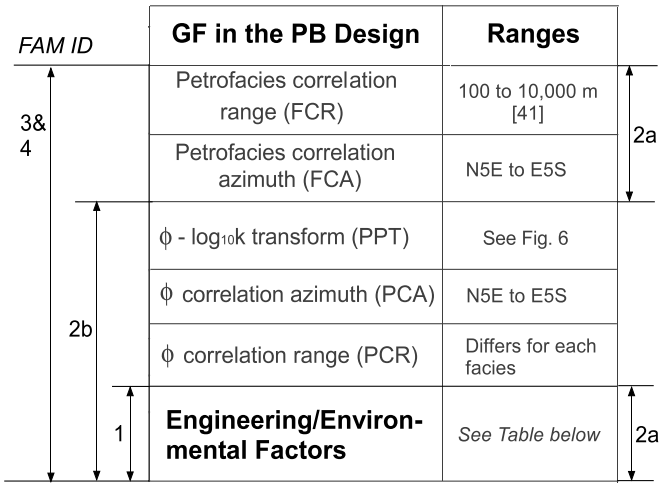

EEF	RPM	RGS	TG	VHR	SAL
- 1	See Fig. 2	0.2	See Fig. 3	See Fig. 4	10,000 ppm
+ 1	See Fig. 2	0.3	See Fig. 3	See Fig. 4	100,000 ppm

Fig. 5. Uncertainty factors and their ranges for each family in the screening (Plackett–Burman) design; −1 = minimum, +1 = maximum; numbers indicate family identification; EEFs are shared by all families; geologic factors are also listed; facies and ϕ correlation range and azimuth are of the lateral direction; azimuth is defined as the direction of maximum correlation projected onto the horizontal plane

They vary only in how porosity and permeability are represented. For each family, the choice and the number of geologic factors depend on the level of designed complexity (Fig. 5). For FAM1 (structural model), because porosity and permeability are assumed homogeneous, the only factors varied are the EEFs. This conceptualization, though unrealistic, provides a baseline for comparing with the complex models in the uncertainty analysis. Subsequently, geologic factors of the families are described.

For FAM2a, four discrete facies were first categorized from analyzing well logs (Yang 2012). A facies model was created using sequential indicator simulation, which conditions the modeled facies to well data. Within each facies, ϕ and k are assumed homogeneous. In addition to the EEFs, two factors controling facies distribution are varied: lateral facies correlation range (FCR) and azimuth (FCA). The range of uncertainty for FCR is determined from those observed for Navajo Sandstone, a Nugget Sandstone equivalent (Hansen 2007). The range of FCA is determined from that modeled for the Nugget Sandstone in Moxa Arch (Li et al. 2011b). Detail of facies modeling, including how facies ϕ and k are determined, can be found in Yang (2012).

FAM2b is a geostatistical petrophysical model without the explicit modeling of facies. In addition to the EEFs, two factors that control ϕ population, i.e., lateral ϕ correlation range (PCR) and azimuth (PCA), are varied. Uncertainty range of PCR is determined by uncertainty in fitting a ϕ variogram model to the experimental variograms using all porosities regardless of facies association. Uncertainty range of PCA follows that of the facies azimuth modeled for FAM2a. Given the variogram parameters, ϕ is populated using sequential Gaussian simulation conditioned to well porosities. Horizontal permeability (k_H) is then populated from porosity using a log-linear transform (PPT) (Nelson 1994). To minimize bias in fitting a single transform to data with a large scatter, PPT is varied as a geologic factor. From the modeled k_H, vertical permeability (k_V) is determined with VHR.

In FAM3, four facies are modeled (the same as FAM2a) before petrophysical properties are modeled within each facies. Facies correlation ranges and azimuths are varied according to their ranges discussed previously. For each facies, ϕ correlation range is varied based on variogram analysis of well log porosities associated with this facies (Yang 2012), while ϕ azimuth adopts the same range as FAM2b. Moreover, the four facies are split into two groups based on their mean porosities. For each group, a set of end member PPT is developed by fitting log-linear transform to core ϕ and k data associated with this group.

In FAM4, in addition to the EEFs and geologic factors of FAM3, facies modeling is constrained by a three-dimensional facies probability cube created from interpolating and extrapolating facies data at well locations. In the study area, two Nugget Sandstone vertical stratigraphic sequences with characteristic ϕ and k are often identified: good-quality upper sand and poor-quality lower deposits (Tillman 1989; Lindquist 1988). These sequences are indeed observed in well logs at the study site (Yang 2012) as well as in nearby Moxa Arch (Li et al. 2011b). A facies probability cube was thus created to honor this trend (how a probability cube can be created from well data to condition facies modeling is described elsewhere (Ma 2009; Ma et al. 2009). Moreover, because Nugget Sandstone cores were collected from various reservoir depths, porosity is observed to decrease with depth due to compaction and cement overgrowth (Houseknecht 1987; Ajdukiewicz and Lander 2010). During porosity modeling, a depth trend is additionally imposed. Therefore, soft data conditioning is accomplished by imposing facies probability cube and porosity-depth trend.

Dynamic Modeling

CO_2 injection is modeled with GASWAT of *Eclipse 300* (Schlumberger 2009), a multiphase compositional simulator. With GASWAT, temperature of the reservoir can vary with depth, which affects phase densities, viscosities, and solubilities. For the two phases (supercritical CO_2-rich phase and H_2O-rich aqueous phase), three components, CO_2, H_2O, and NaCl, are modeled. Gas-aqueous equilibrium is modeled through an equation of state, and solubility correction is made to reflect the effect of salinity on CO_2 solubility. Initial reservoir pressure is set hydrostatic, with a reference pressure of 37.3 MPa at 3,658-m depth. Aquifer temperature is assigned according to TG, which is varied in the uncertainty analysis. Model boundaries are represented by a Carter-Tracy external aquifer of large radius and thickness, which ensures an open boundary that allows formation brine, and later CO_2, to flow out (*Eclipse 300* records brine leakage from the model into the external aquifer). Model is thus considered part of a larger semi-infinite system, consistent with site understanding. Simulations were conducted setting the western boundary to no flow, which did not significantly impact CO_2 predictions. Flow is generally not influenced by boundary conditions if boundaries lie far from the center of disturbance (Carrera and Neuman 1986). CO2STORE, another *Eclipse 300* module, is not used due to its temperature and pressure limits, which this model exceed due to the greater injection depth. Also, the equation of state in CO2STORE cannot account for the variation of reservoir temperature with depth.

For all model families, a single injector injects CO_2 for 50 years. It fully perforates the formation at 3,658–3,840 m, comparable to the injection depth of Li and Zhang (2014) (4,236 m). To prevent hydraulically fracturing the formation, an injector bottomhole

pressure (BHP) constraint is set at 1.8 times hydrostatic pressure (Li et al. 2011b). With this constraint, a fixed mass injection rate of 1/3 Mt/year is achieved from numerical experimentation, which reveals that the injection rate is largely constrained by the lower end member of PPT. For the given boundary conditions and the permeability range varied, a rate higher than 1/3 Mt/year can cause the injector BHP of some models (with lower mean permeabilities) to exceed the constraint, which prompts *Eclipse* to reduce the rate. This would create an issue as different amounts of CO_2 would be injected by the model families, making their comparison difficult.

As a result of the open boundaries and the relatively low injection rate, pressure buildup in the model is modest and is not evaluated. A constant rate is thus maintained by all models, leading to the same injected CO_2 (17 Mt over 50 years). To achieve a higher rate, multiple injectors are needed and the associated pressure buildup can be controlled by brine production (Li et al. 2011a). Because the long-term fate of CO_2 is of interest, a postinjection phase is modeled for 1,950 years, for a total simulation time of 2,000 years. Sufficient time thus allows CO_2 to migrate from the injector, and the effect of large-scale permeability heterogeneity on migration and trapping can be evaluated. All simulations are checked for accuracy and convergence before results are analyzed. For each family, parameters important to predicting brine leakage, trapped gas, dissolved gas, and CO_2 storage ratio are identified, while uncertainty in CO_2 storage is assessed by the RS models. The analysis is carried out at selected output times including 2041, 2061 (end of injection), 2310, 2810, 3210, 3610, and 4010 (end of simulation) (Year 2011 is the start of simulation).

Uncertainty Analysis

Because Li and Zhang (2014) provides a recent review of the DoE and RS method, only an overview is presented here. A screening SA is conducted first by varying a subset of the uncertain input factors simultaneously according to a design table (Montgomery 2008). The factors varied can be continuous or categorical, the latter typically reflecting modeling choices. Results of the SA are examined with multivariate analysis of variance (MANOVA), which identifies and ranks the factors that exert statistically significant effects on a simulation outcome. Though a variety of designs are available (the same design can be used for analyzing multiple outcomes), a two-level Plackett–Burman (PB) design, a useful screening tool to help identify the most significant uncertainty factors with the fewest number of simulation runs (Milliken et al. 2007), is adopted here. After the screening analysis, RS modeling consists of fitting an analytical function to a simulation outcome (Myers and Montgomery 1995). This function is generated by running simulations according to an RS design using factors identified by the screening design as the most important for predicting that outcome at a user-specified significance. A central composite design is used here, which requires three values for each factor, i.e., $-/0/+$ (low/median/high). These values can correspond to key probabilities, although it is not a requirement. To obtain the RS model, a quadratic polynomial function, which is found accurate and robust in analyzing different reservoir problems (Peng and Gupta 2004; Yeten et al. 2005), is fitted to the simulation outcome via multilinear regression. Although alternative designs and fitting methods are available, the best design and fit are problem dependent. In general, researchers rely on verification to test the robustness of a chosen design in replicating simulated values at non-RS-design points. In this paper, the RS models are verified at PB design points, which lie on parameter space boundary. According to Peng and Gupta (2004), such "extreme test runs" can exaggerate RS errors, although this decision can lead to significant computational savings. After the verification, the RS model is considered a proxy for reservoir simulation, i.e., a statistically based predictive model between important input factors and simulation outcome (response). With the RS model, a Monte Carlo simulation (MCS) is carried out by randomly drawing the factors according to their respective probability density functions (PDFs), which leads to a PDF of the outcome. This analysis is orders of magnitude faster than one based on full-physics simulations. In the MCS, however, factor PDFs must be drawn from the same ranges in which the RS model is verified. At this study site, information on exact parameter PDFs is lacking. A Gaussian distribution is assumed for most factors, i.e., $[-1, +1]$ parameter ranges correspond to a 99% probability. An exception is the relative permeability model for which equal probability (i.e., a uniform distribution) is assigned to the end members. The DoE and RS analysis is performed with *JMP 9.0* of Statistical Analysis Software.

In this paper, geologic factors and EEFs are varied according to experimental designs (Fig. 5), which directly influence the building of the site model. Because the number of geologic factors increases with model complexity, the number of simulations required by the designs increases accordingly. For all families, model building is first dictated by the PB design, which specifies a number of simulation runs: 13 (FAM1, FAM2a, FAM2b) and 21 (FAM3 and FAM4). For FAM4, soft data conditioning is incorporated into the model building procedure, but not into the PB design, which is identical to that of FAM3. The effect of data conditioning is evaluated by comparing the uncertainty outcomes of FAM3 (no conditioning) with FAM4. The PB design for generating the FAM4 models is shown in Table 1 [designs of the other families can be found in Yang (2012)]. For each family, after the screening analysis identifies a list of important factors, an RS design is generated using these factors to develop a proxy model for CO_2 storage. The RS designs are typically of higher resolutions and more simulations are needed (see "Results"). In these simulations, as long as geologic factors are identified as important, additional static models incorporating variations of such factors must be built. Despite the computational efficiency of the uncertainty method,

Table 1. PB Design for FAM4

Run	FCA	FCR	PCA	PCR	PPT	VHR	SAL	RGS	RPM	TG
1	1	1	1	−1	1	−1	1	−1	−1	−1
2	1	1	1	1	−1	1	−1	1	−1	−1
3	1	−1	1	−1	1	−1	−1	−1	−1	1
4	−1	−1	−1	−1	1	1	−1	−1	1	−1
5	0	0	0	0	0	0	0	0	0	0
6	−1	−1	1	−1	−1	1	1	1	1	−1
7	−1	−1	1	1	1	1	−1	1	−1	1
8	1	−1	−1	−1	−1	1	1	−1	−1	1
9	−1	−1	−1	1	1	−1	−1	1	−1	−1
10	1	1	−1	−1	1	−1	−1	1	1	1
11	−1	1	−1	−1	1	1	1	1	−1	1
12	−1	1	1	−1	−1	1	−1	−1	1	1
13	1	1	−1	1	−1	1	−1	−1	−1	−1
14	−1	1	−1	1	−1	−1	−1	−1	1	1
15	1	−1	−1	1	1	1	1	−1	1	−1
16	−1	−1	1	1	−1	−1	1	−1	−1	1
17	−1	1	1	1	1	−1	1	−1	1	−1
18	−1	1	−1	−1	−1	−1	1	1	−1	−1
19	1	−1	1	−1	−1	−1	−1	1	1	−1
20	1	−1	−1	1	−1	−1	1	1	1	1
21	1	1	1	1	1	1	1	1	1	1

Note: $-1/0/1$ indicate different values assigned to an uncertain input factor.

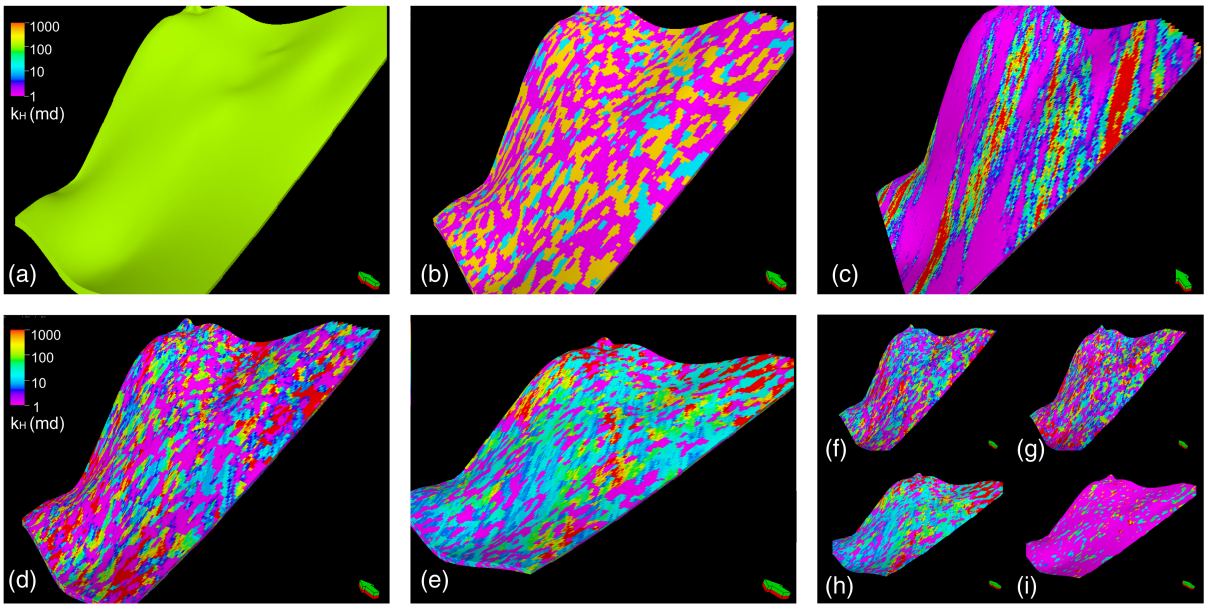

Fig. 6. Realization of k_H for each family; arrow points north: (a) FAM1; (b) FAM2a; (c) FAM2b; (d) FAM3; (e) FAM4; (f) first layer of FAM3; (g) last layer of FAM3; (h) first layer of FAM4; (i) last layer of FAM4

a large effort is devoted to building the static models and conducting CO_2 simulations with these models.

A realization of k_H for each model family is shown (Fig. 6), corresponding to the center run of the respective PB design, i.e., all factors assume median values. Given the varying support data and modeling choices, different permeability heterogeneities are created. For example, FAM2a exhibits facies variation, while within-facies permeability is homogeneous. Permeability of FAM2a, FAM2b, and FAM3 are statistically homogeneous without significant trends. Compared with FAM3, where mean permeability does not vary areally or with depth, good-quality layers with higher permeabilities are observed in the upper model region of FAM4 because of facies conditioning. Also, due to the porosity-depth trend, k_H of FAM4 decreases with depth, an effect absent in the other families. Fig. 6, however, only illustrates the difference in mean heterogeneity representation by the families. Additional variability exists *among* the models of each family because geologic factors are varied according to experimental designs.

Results

Results are presented in four subsections: (1) screening test outcomes, (2) RS modeling and verification, (3) Monte Carlo simulation assessing CO_2 storage uncertainty, and (4) representative plume footprints for each family selected from RS model runs corresponding to end member SRs. Fig. 5 contains meanings of the acronyms representing the uncertainty factors.

Screening Tests

Screening test results of all families are examined at end of injection (EOI) and end of simulation (EOS) (Table 2). At a given output time and for a given outcome, *t*-ratio of each family is used to determine and rank the effect of each uncertainty factor on influencing the outcome. As a key statistic of MANOVA, *t*-ratio is defined as ratio of variance of the response caused by a given factor to that due to all experiments (Montgomery 2008). When the outcome is CO_2 storage ratio at EOS, a *t*-ratio-based ranking is shown in Fig. 7 for FAM4. The same analysis was conducted for all other outcomes and for all families.

Results of each family are first examined at different times. For FAM4, over the entire simulation time, PPT, FCR, FCA, and VHR are the four most important factors impacting brine leakage, suggesting that this outcome is controlled by aquifer permeability that determines fluid pressure evolution, which in turn controls leakage. In predicting residual gas, results at EOI are different from those at EOS: (1) RPM and TG are the most important

Table 2. Significant Factors Identified by the PB Design for Each Family That Impact Different Outcomes: Brine Leakage, Residual Gas, Dissolved Gas, and CO_2 SR

Simulation outcomes	End of injection	End of simulation
Brine leakage		
FAM1	RPM/SAL	RPM/SAL
FAM2a	FCR	FCR
FAM2b	PPT/PCA	PPT
FAM3	PPT	PPT
FAM4	PPT/FCR/FCA/VHR	PPT/FCR/FCA/VHR
Trapped (residual) gas		
FAM1	TG	SAL/RPM/RGS
FAM2a	RPM	RGS/SAL/RPM
FAM2b	RPM/PPT/RGS	PPT/SAL/PCA/RGS
FAM3	RPM/PPT	PPT/RGS
FAM4	RPM/PPT/RGS/TG	PPT/SAL/FCR/RGS
Dissolved gas		
FAM1	SAL/RPM/TG	SAL/RPM/VHR
FAM2a	SAL	SAL
FAM2b	PPT/SAL/TG/RPM/PCA	PPT/SAL
FAM3	PPT/SAL	PPT/PCA
FAM4	PPT/SAL/FCR	PPT/FCR/SAL
SR		
FAM1	TG	SAL
FAM2a	RPM	VHR
FAM2b	PPT/TG	PPT/RGS
FAM3	PPT/RPM	PPT/RPM
FAM4	PPT/RPM/RGS	PPT/FCR/RGS

Note: Significance level = 90%.

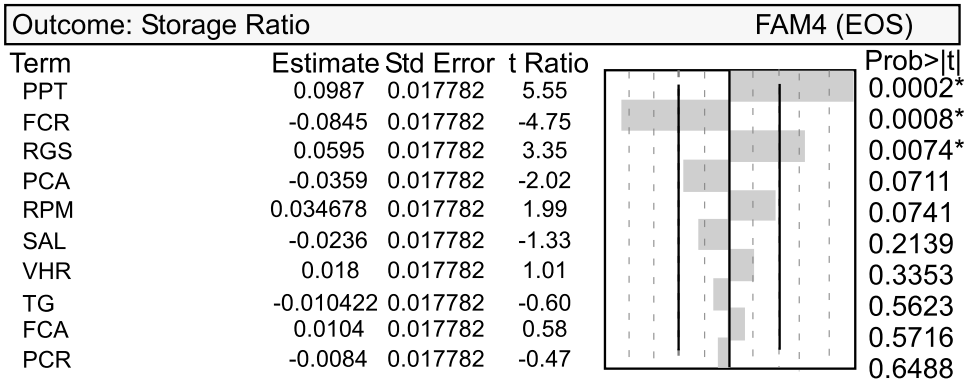

Fig. 7. Example screening analysis result for FAM4 at 90% significance (bold lines); outcome is CO_2 storage ratio at the end of simulation; statistically significant factors include ϕ-kH transform, facies correlation range, and residual gas saturation; negative t-ratio means varying the value of a factor from -1 to $+1$ reduces the storage ratio

factors during injection, but become unimportant by EOS; (2) during postinjection, PPT and FCR exert a dominant effect, which can be explained by their influence on formation mean k and its connectivity. Higher mean k and greater lateral continuity of high-k facies can contribute to more lateral plume spreading and more brine is in contact with gas, which leads to more residual trapping during imbibition. Because supercritical CO_2 migrates continuously along the inclined aquifer, the same two factors are consistently important over time. In predicting dissolved gas, PPT and FCR are also the most important: more lateral spreading causes more gas to contact brine and more dissolution.

Comparing brine leakage among the families, the important factor(s) remain the same over time (before and after injection), which suggests that sensitivity for predicting leakage is not strongly affected by time. In predicting residual gas, results differ among families to some degree: for FAM2, FAM3, and FAM4, RPM is important by the EOI, but becomes unimportant by the EOS; for FAM1, TG is important during injection, but is not after injection ceases. In predicting dissolved gas, factors that influence plume spreading become more important with increasing time: in FAM3 and FAM4, by the EOS, PCA and FCR become more important than SAL.

Results are compared across the families at the same time. As model complexity increases, for the same outcome geologic factors that determine aquifer k (i.e., mean value and connectivity) become increasingly important, especially by the end of simulation. For FAM1 and 2a, at any output time, the important factors are mostly EEFs, as expected. When FAM2b, 3, and 4 are examined, PPT is dominantly important for predicting all outcomes at all times. When complexity is built into the model reflecting increasing site knowledge, geologic factors exert a dominant effect on predictions, while EEFs become less important. For the simple families, RPM and RGS are identified as key factors. However, as model complexity increases these give way to PPT and FCR.

RS Modeling of Storage Ratio

For a given family, after PB design identifies a list of important factors, an RS design is generated based on these factors to develop a proxy model for predicting CO_2 storage. Factors included in the RS design are the union of all important factors for predicting the SR at both times. For example, if PPT is not important with regards to predicting residual gas but is important with regards to predicting dissolved gas, it is included in the design because both forms of CO_2 contribute to the SR. Moreover, if PPT is not important at EOI but becomes important at EOS, it is included as well. For FAM1, the important factors for predicting residual and dissolved gases over both time scales are TG, SAL, RPM, VHR, and RGS (Table 2), which yield 44 simulations based on the central-composite design (Yang 2012). Compared with the PB design, more simulations are needed because RS designs are generally of higher resolution. For the other families, the number of RS simulation runs are 44 (FAM2a), 46 (FAM2b), 44 (FAM3), and 80 (FAM4).

For the storage ratio, an RS model is fitted to the simulated storage ratio at each output time: 2041, 2061 (EOI), 2310, 2810, 3210, 3610, and 4010 (EOS). For example, 44 SRs are exported from FAM1's RS design runs at year 2041, with which one RS model is created. For the entire simulation time, seven storage ratio RS models are created for this family. These models are verified by comparing the RS-model-predicted SR to the simulated SR at PB design points, which yields small errors (Table 3), i.e., means of the RS errors are close to 0.0, standard deviations are generally small, and error distributions are frequently symmetric around the means (see Fig. 8 for FAM4). Also, had the verification points been selected internal to the parameter space, the RS error is expected to be smaller (Peng and Gupta 2004). The RS models are considered adequate proxy models for the Monte Carlo analysis.

Table 3. Summary Statistics of the RS Errors at PB Design Points

Family identification	RS error at the EOM [minimum, mean, maximum, standard deviation]	RS error at the EOM [minimum, mean, maximum, standard deviation]
FAM1	$[-2.1 \times 10^{-1}, 1.0 \times 10^{-4}, 2.1 \times 10^{-1}, 1.3 \times 10^{-1}]$	$[-3.5 \times 10^{-2}, 1.0 \times 10^{-2}, 5.0 \times 10^{-2}, 2.0 \times 10^{-2}]$
FAM2a	$[-5.5 \times 10^{-1}, -4.0 \times 10^{-2}, 1.6 \times 10^{-1}, 1.6 \times 10^{-1}]$	$[-8.2 \times 10^{-2}, 1.0 \times 10^{-3}, 1.1 \times 10^{-1}, 4.0 \times 10^{-2}]$
FAM2b	$[-5.4 \times 10^{-1}, -4.0 \times 10^{-2}, 3.0 \times 10^{-2}, 1.5 \times 10^{-1}]$	$[-1.6 \times 10^{-1}, -9.0 \times 10^{-3}, 8.8 \times 10^{-2}, 6 \times 10^{-2}]$
FAM3	$[-1.2 \times 10^{-1}, -9.6 \times 10^{-3}, 5.0 \times 10^{-2}, 4.0 \times 10^{-2}]$	$[-3.6 \times 10^{-1}, -4.0 \times 10^{-2}, 1.7 \times 10^{-1}, 1.5 \times 10^{-1}]$
FAM4	$[-5.2 \times 10^{-1}, -4.0 \times 10^{-2}, 4.0 \times 10^{-2}, 1.2 \times 10^{-1}]$	$[-1.9 \times 10^{-1}, -2.0 \times 10^{-2}, 7.0 \times 10^{-2}, 6.0 \times 10^{-2}]$

Note: Error = RS-model-predicted storage ratio − simulated storage ratio at PB design point.

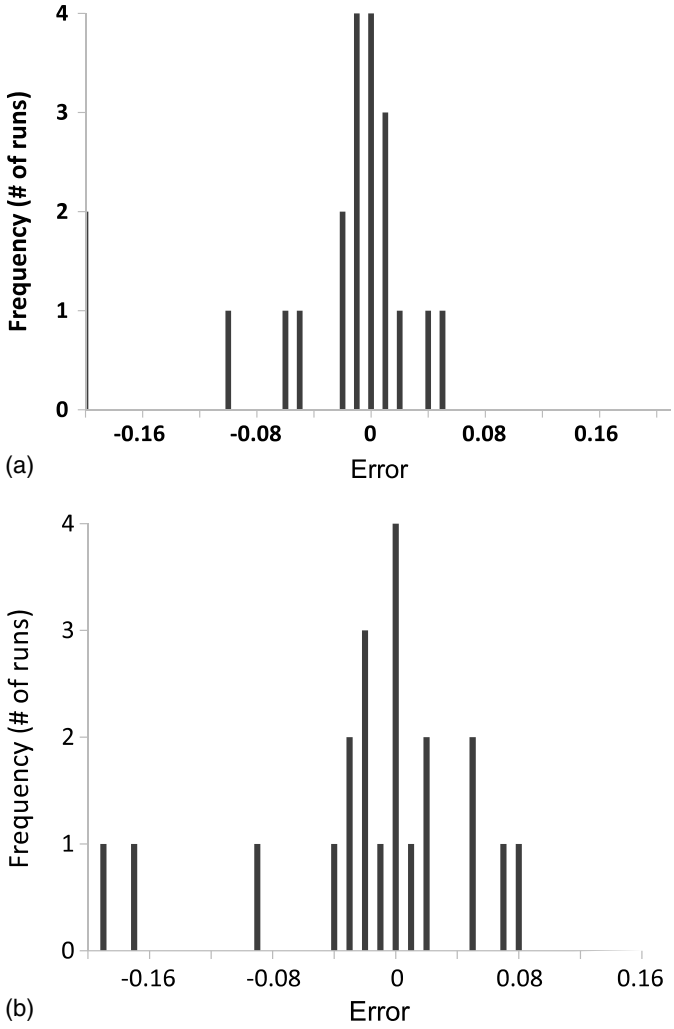

Fig. 8. Verification of the RS models for FAM4: (a) EOI; (b) EOS

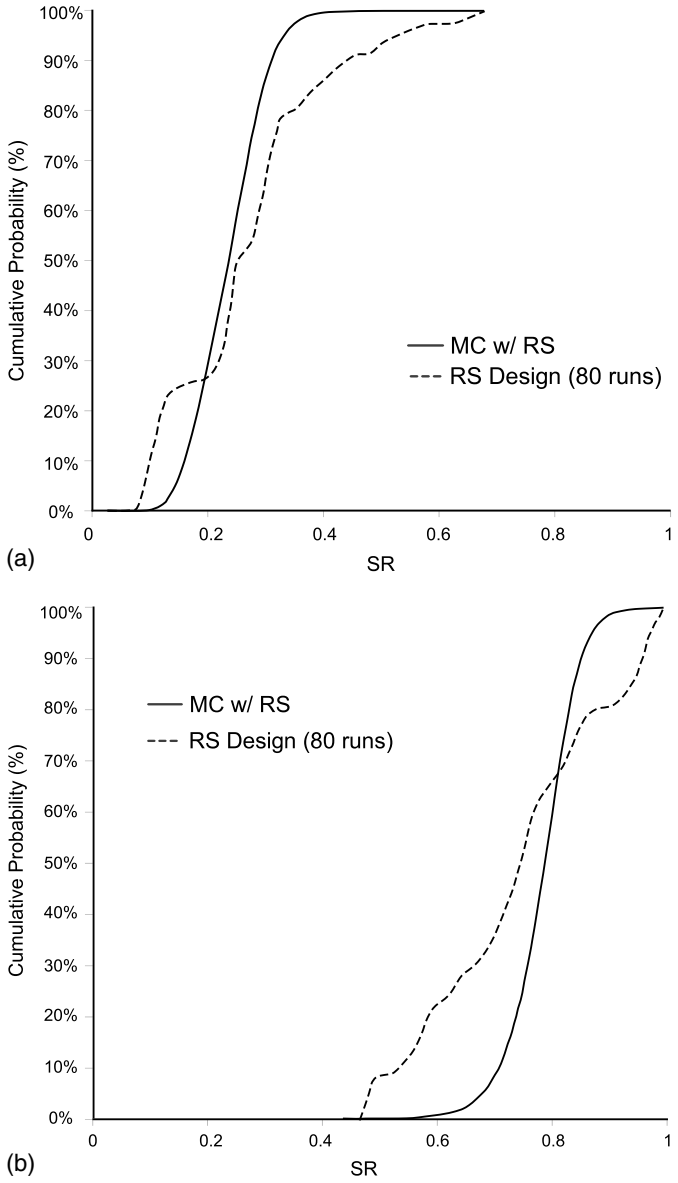

Fig. 9. CDF of the storage ratio for FAM4: (a) EOI; (b) EOS; MC with RS is generated with 500,000 MC simulations using the RS model (exhaustive CDF); RS design is CDF constructed using results from the 80 RS runs for this model family

Monte Carlo Analysis

For each family, RS models created at seven output times are used to assess storage ratio uncertainty. Five hundred thousand Monte Carlo simulations are run, randomly sampling the input factors (i.e., axes of the RS model) according to their PDFs. Each random drawing of a vector of the input factors gives rise to one RS-predicted storage ratio. After 500,000 simulations, which took less than 2 min on a PC workstation, a cumulative distribution function (CDF) of the SR can be created (Fig. 9 for FAM4; solid line). It would take hundreds of years if this analysis were conducted with the reservoir simulator, assuming that one simulation can be completed overnight. Clearly, here lies the chief strength of the DoE and RS method because the same analysis with full-physics simulations is impractical.

From the CDFs of the storage ratio (one at each output time), a prediction envelope can be created and further compared among the families (Fig. 10). Given the uncertainty in parameters and modeling choices, the SR exhibits a considerable spread: at EOI, it ranges from 0.18 to 0.38; at EOS, 0.71 to 0.99. At a given output time, uncertainty in SR for FAM2b, FAM3, and FAM4 are larger than those of FAM1 and FAM2a, likely because the former models contain more uncertainty factors contributing to greater prediction uncertainty. Uncertainty in SR also changes with time. By EOI, prediction envelopes of all families are more or less similar: where plume migration is limited, heterogeneities near the injector are not significantly different among the families, thus similar SR uncertainty. After injection ceases, prediction envelope of each family deviates gradually from one another, reflecting different (evolving) large-scale heterogeneity experienced by each family because plume migrates continuously along dip. Clearly, uncertainty in predicting CO_2 storage is affected by conceptual model, the number of factors evaluated, and time. When comparing mean and range of the SR, prediction envelope of FAM3 is the closest to FAM4, while all other families estimate higher means (the simpler the model, the greater the mean). In this case, increasing reservoir heterogeneity leads to less storage, likely due to reduced sweep efficiency (Deng et al. 2012).

Because RS models contain errors, they are imperfect representations of the true but unknown prediction space. For a given problem, RS errors depend on the RS design and fitting method.

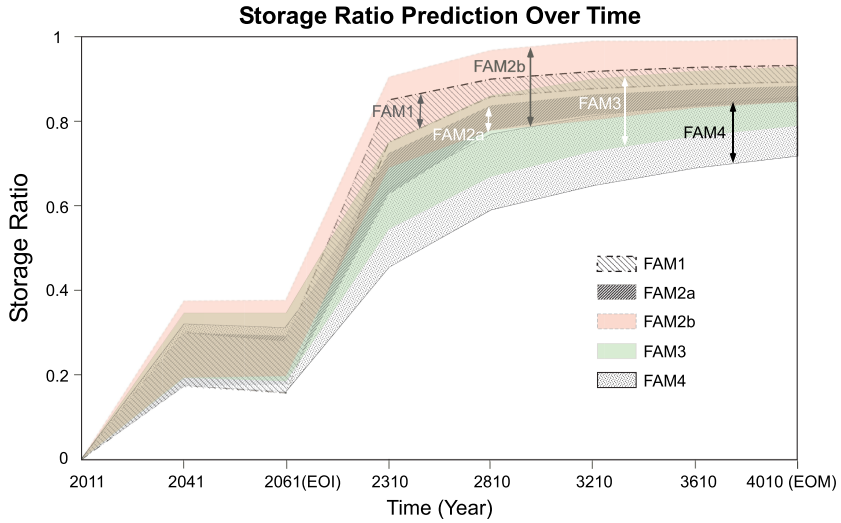

Fig. 10. Prediction envelope of the RS-model-predicted storage ratio over time; for each family, prediction envelope (at a given time) is defined by [P10, P90] of the storage ratio CDF; between output times, the envelopes are created from linear interpolation

In general, error decreases with increasing resolution of the design (not tested here), but more simulation runs are needed. The MC-predicted storage ratio CDFs are therefore approximations whose precisions may change with available computing resources.

Plume Footprint

From the RS design runs, a nonexhaustive CDF of the storage ratio is constructed, e.g., Fig. 9 (dashed line). Compared with the exhaustive CDF, the nonexhaustive CDF is less smooth because parameters sampled by these runs are discontinuous. However, the nonexhaustive CDF has largely captured the range of the exhaustive CDF, suggesting that representative outcomes other than SR may be identified from these runs. One outcome of interest is the footprint of supercritical CO_2 (both residual and mobile gas), which is defined here as the model layer with the largest plume. When SR is at its highest (i.e., greatest dissolution and residual trapping), CO_2 footprint tends to be more laterally extensive, and vice versa (Sifuentes et al. 2009; Liu and Zhang 2011). Therefore, representative plume footprints are identified by visualizing the RS design runs corresponding to minimal, median, and maximum SRs in the nonexhaustive CDF (Fig. 11 at the EOI; Fig. 12 at the EOS).

For FAM1 and 2a, at both EOI and EOS, representative plumes at minimal, median, and maximum SRs are not as drastically different from one another as those of FAM2b, 3, and 4, consistent with the observation that for the former families, their SR uncertainty ranges are comparatively small. For FAM2b, 3, and 4, however, the differences are much more pronounced: gas plume corresponding to minimum SR stays close to the injector and does not travel far, resulting in minimum dissolution and residual trapping, while that corresponding to maximum SR migrates far from the injector, which explains why PPT is always dominantly important for these families. PPT determines the average reservoir permeability, and the higher this permeability, the faster the CO_2 can migrate, thus more gas dissolution and trapping occur per unit time. For FAM4, at its maximum SR (~1), little residual and mobile gas remains by EOS [Fig. 12(o)]. When the corresponding parameters are examined, mean permeability is high and salinity is low. Gas plume spreads widely and quickly and is mostly dissolved by EOS.

Discussion

Uncertainty in modeling CO_2 storage is commonly evaluated with a fixed conceptual model varying only EEFs. Within such a framework, factors such as relative permeability are often identified as important. In this study, GCS in an inclined aquifer is of interest, and uncertainty in building the site model (i.e., k heterogeneity) dominates CO_2 predictions over that due to the variation of EEFs. Because k can vary over several orders of magnitude in a single aquifer, uncertain geologic factors influencing its magnitude, orientation, and connectivity can induce large changes in the permeable pathways through which CO_2 migrates. For example, permeability magnitude influences the speed of gas migration, reservoir fluid pressure, and brine leakage. For families in which heterogeneity is explicitly modeled, porosity-permeability transform and facies correlation structure are found to significantly influence storage: the former factor influences permeability magnitude, the latter permeability connectivity. These effects are magnified in an inclined aquifer, where a runaway plume can occur: as CO_2 migrates continuously along dip, different large-scale heterogeneities (as represented by different model families) are continuously experienced by the plume, which influences its trapping and storage. On the other hand, parameters such as RPM and RGS vary only within 1 or 2 orders, and compared with conceptual uncertainty in modeling heterogeneity, they exert far less influence on CO_2 predictions. The previous results are further compared with Li and Zhang (2014), where the same formation in a neighboring region was evaluated. There, because of the lack of significant dip, CO_2 was observed to aggregate near the injector and conceptual uncertainty was found to be much less important. And, for a similar time scale evaluated, relative permeability was identified as the most significant factor. Thus, the notion that relative permeability exerts a dominant control on CO_2 storage is likely true when aquifer dip angle is small. To determine whether the previous insights can apply to other sites, different storage systems need to be examined, e.g., porous versus fractured rocks, nonreactive versus reactive systems, shallow versus deep injection, and sluggish versus strong background flow. In evaluating these systems, factors specific to each site need to be selected. Again, DoE and RS method provides a promising approach for these analyses.

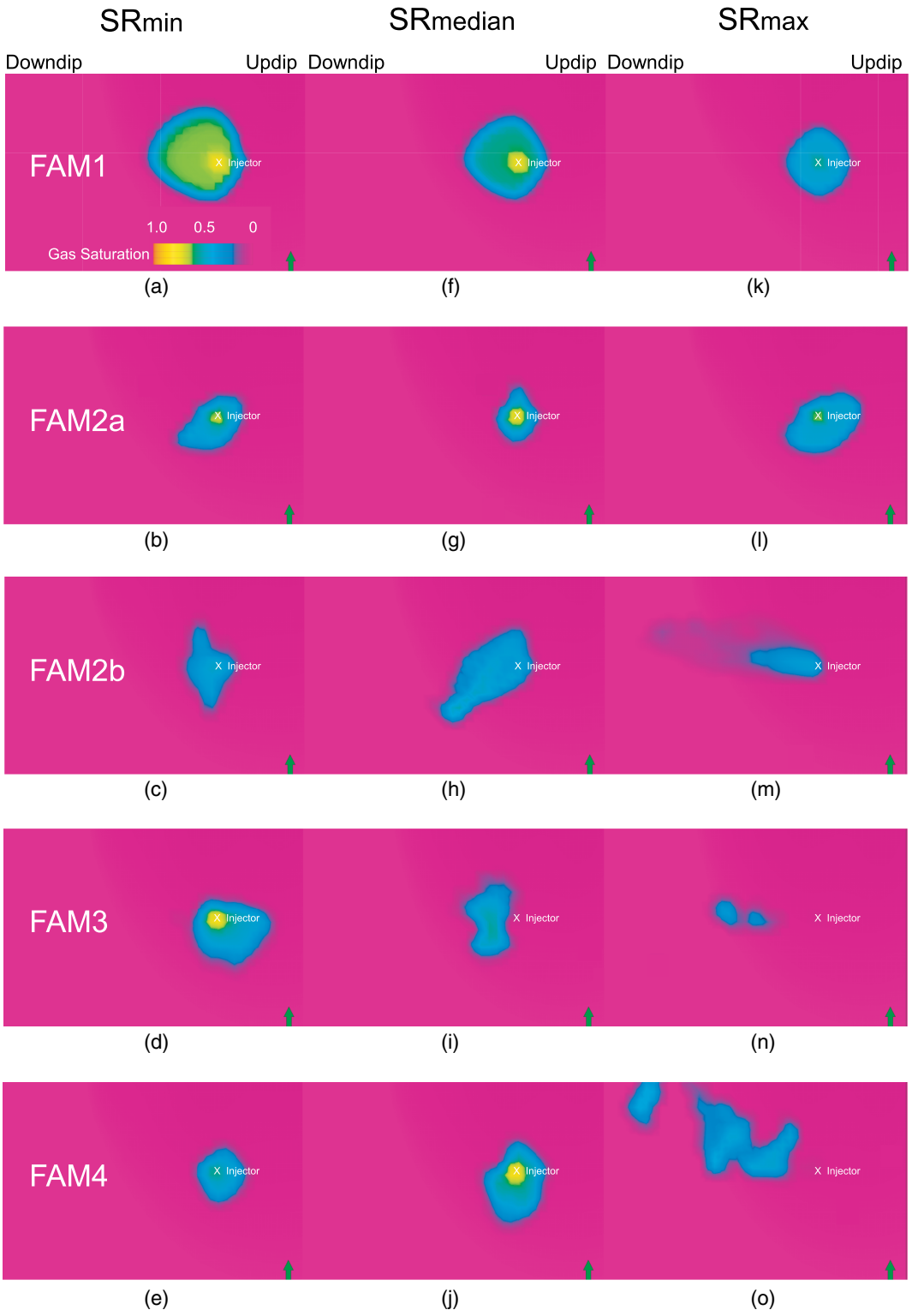

Fig. 11. Gas saturation (mobile+residual supercritical CO_2) predicted by each family at end of injection: minimum SR for (a) FAM1; (b) FAM2a; (c) FAM2b; (d) FAM3; (e) FAM4; median SR for (f) FAM1; (g) FAM2a; (h) FAM2b; (i) FAM3; (j) FAM4; maximum SR for (k) FAM1; (l) FAM2a; (m) FAM2b; (n) FAM3; (o) FAM4; arrow points north

In site assessment, besides CO_2 storage, leakage is also an important concern. In Li and Zhang (2014), gravity-stable flow was simulated under conditions of cool formation temperatures and high formation fluid pressures, suggesting that deep injection may lead to reduced leakage risk. In this paper where CO_2 is injected at a similar depth, gas plume is also observed to migrate downdip under similar temperature and pressure conditions. In both studies, mixture densities predicted by GASWAT were inspected. Under suitable conditions, the supercritical CO_2-rich phase (containing a small amount of H_2O) was found to have higher mixture densities than the H_2O-rich brine phase (with a small amount of CO_2). In Lu et al. (2009), when a different equation of state is

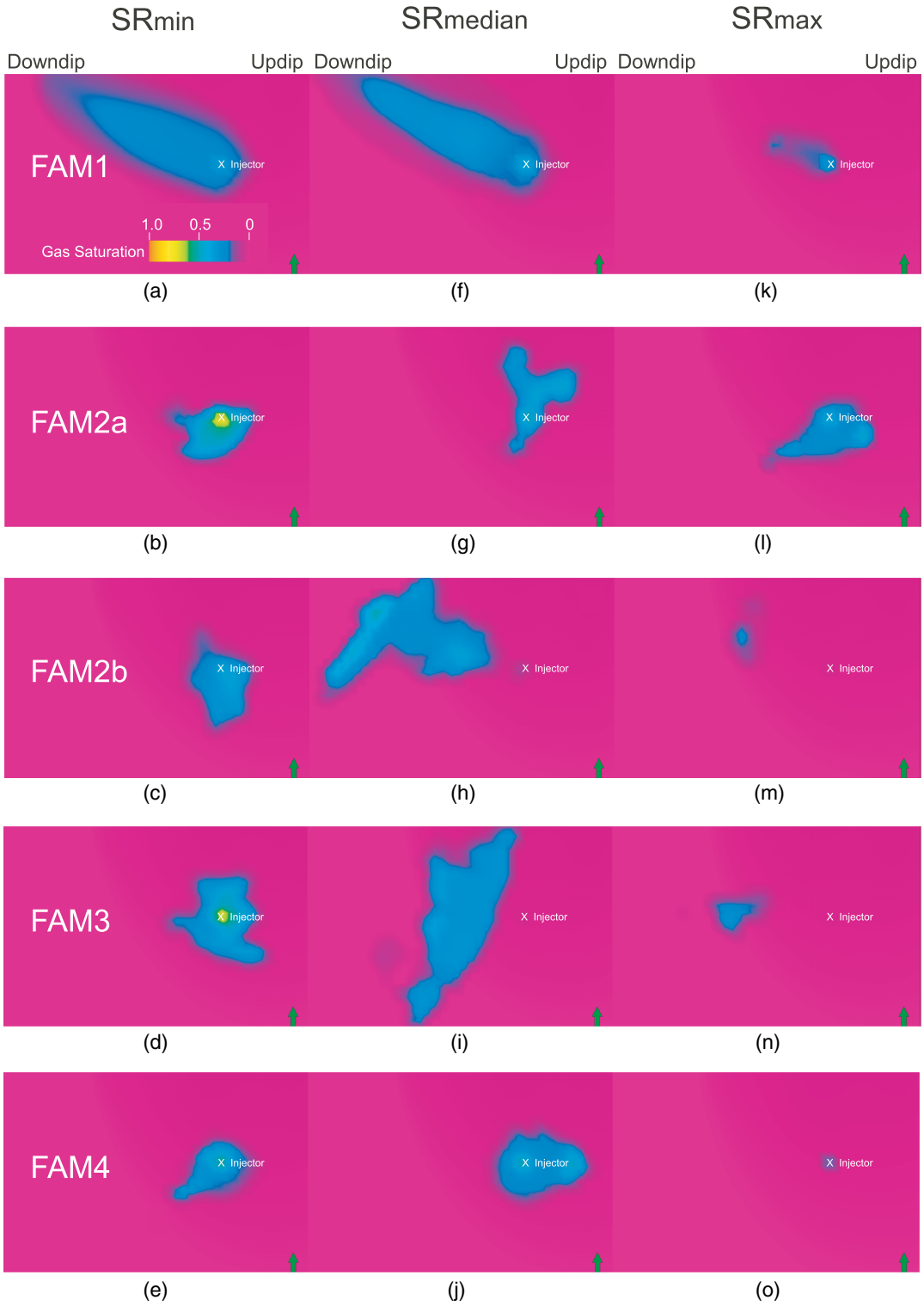

Fig. 12. Gas saturation (mobile+residual supercritical CO_2) predicted by each family at end of simulation: minimum SR for (a) FAM1; (b) FAM2a; (c) FAM2b; (d) FAM3; (e) FAM4; median SR for (f) FAM1; (g) FAM2a; (h) FAM2b; (i) FAM3; (j) FAM4; maximum SR for (k) FAM1; (l) FAM2a; (m) FAM2b; (n) FAM3; (o) FAM4; arrow points north

implemented, CO_2 dissolution can cause brine to become less dense. In Firoozabadi and Cheng (2010), under sufficiently high pressure, "CO_2 density can be higher than water density." However, mixture density calculation is subject to uncertainty. If GASWAT's prediction of mixture densities is adequate for the range of temperature and pressure conditions encountered in the authors' studies, gravity-stable migration then becomes possible. Future work will evaluate alternative equations of state that will be constrained by experiments with conditions applicable to these deep systems. Moreover, while downdip flows are observed, a few simulations predict updip migration when a higher TG is assigned, e.g., median SR in FAM4 (Fig. 12). Reduced uncertainty in aquifer temperature

is also needed to evaluate whether gravity-stable migration is a likely scenario.

Conclusion

In modeling CO_2 storage in a deep inclined aquifer, the impact of geologic, engineering, and environmental uncertainty factors on parameter importance and prediction uncertainty is evaluated. By building and simulating four increasingly complex geologic model families, the effect of permeability representation is investigated. Over 50 years, 17 Mt of CO_2 is injected at a depth of approximately 3,750 m. Postinjection modeling extends the total simulation time to 2,000 years. Using design of experiment, a screening sensitivity analysis is first conducted for all model families, systematically varying uncertain input parameters. Parameters that have first-order impact on CO_2 predictions (i.e., trapped gas, dissolved gas, brine leakage, storage ratio) are identified. A response surface analysis then generates accurate proxy models for predicting CO_2 storage, with which uncertainty in the storage ratio is quantified. A set of insights are summarized as follows:

- For the inclined aquifer, conceptual uncertainty and the associated geologic factors can dominate the prediction of CO_2 storage. When model is of low complexity, the most important parameters influencing various predictions are engineering and environmental factors. When model increases in complexity, geologic factors become more important. For a given model family, the important parameters can change with time.
- Uncertainty in the predicted CO_2 storage varies with time. The storage ratio is 0.18–0.38 at the end of injection and 0.71–0.99 at the end of simulation. Over longer times, this uncertainty deviates gradually among the model families, reflecting different large-scale heterogeneity as experienced by each family because plume migrates continuously along dip.
- Gravity-stable flow in deep (≥3,750 m) formations is possible under conditions of low formation temperatures and high formation fluid pressures. Greater injection depth, though more expensive, offers greater storage security and enhanced storage capacity.
- Uncertainty analysis can be conducted efficiently with the DoE and RS method. It took only minutes to obtain the storage ratio CDF using Monte Carlo simulations with the RS model.
- Formation dip can significantly impact uncertainty outcomes. Because the family incorporating all available hard and soft data is considered the most realistic, resources should be devoted first to characterize geologic factors such as porosity-permeability transform and facies correlation structure. For aquifers with gentle incline, relative permeability model appears more important (Li and Zhang 2014).

This study can serve as an analog for deep aquifers in basins where connections to the shallow subsurface exist. The method of evaluating multiple conceptual models can be applied to other data-poor settings where key characterization targets need to be identified. If CO_2 injection is carried out in the future, RS-based history matching (Amudo et al. 2008) can be performed to reduce current conceptual uncertainty, leading to more accurate models.

Acknowledgments

Funding for this study was provided by NSF (EAR-0838250) awarded to the first author. We acknowledge the donation of software (Petrel, Petrophysics Interactive, Eclipse) from Schlumberger, Inc. We also acknowledge detailed comments from two anonymous reviewers, which lead to improved organization and clarity of this paper.

References

Ajdukiewicz, J. M., and Lander, R. H. (2010). "Sandstone reservoir quality prediction: The state of the art." *AAPG Bull.*, 94(8), 1083–1091.

Amudo, C., Graf, T., Harris, N. R., Dandekar, R., Ben Amor, F., and May, R. S. (2008). "Experimental design and response surface models as a basis for stochastic history match—A Niger Delta experience." *IPTC 2008;(12665): Int. Petroleum Technology Conf.*, Kuala Lumpur, Malaysia.

Bachu, S. (2003). "Screening and ranking of sedimentary basins for sequestration of CO in geological media in response to climate change." *Environ. Geol.*, 44(3), 277–289.

Bandilla, K., Kraemer, S. R., and Birkholzer, J. T. (2012). "Using semi-analytic solutions to approximate the area of potential impact for carbon dioxide injection." *Int. J. Greenhouse Gas Control*, 8(5), 196–204.

Beni, A. N., Clauser, C., and Erlstrom, M. (2011). "System analysis of underground CO_2 storage by numerical modeling for a case study in Malmo." *Am. J. Sci.*, 311(4), 335–368.

Bennion, B., and Bachu, S. (2006a). "The impact of interfacial tension and pore-size distribution/capillary pressure character on relative permeability at reservoir conditions in -Brine systems." *SPE 99325*, Society of Petroleum Engineers of Europec/EAGE, Vienna, Austria.

Bennion, B., and Bachu, S. (2006b). "Supercritical and s-brine drainage and imbibitions relative permeability relationships for intergranular sandstone and carbonate formations." *SPE 99326*, Society of Petroleum Engineers of Europec/EAGE, Vienna, Austria.

Benson, S. (2006). "Relative permeability explorer beta." ⟨http://pangea.stanford.edu/research/bensonlab⟩ (Mar. 10, 2010).

Carrera, J., and Neuman, S. P. (1986). "Estimation of aquifer parameters under transient and steady state conditions: 3. Application to synthetic and field data." *Water Res. Res.*, 22(2), 228–242.

Deng, H., Stauffer, P. H., Dai, Z., Jiao, Z., and Surdam, R. C. (2012). "Simulation of industrial-scale CO_2 storage: Multi-scale heterogeneity and its impacts on storage capacity, injectivity and leakage." *Int. J. Greenhouse Gas Control*, 10(9), 397–418.

Firoozabadi, A., and Cheng, P. (2010). "Prospects for subsurface sequestration." *Am. Inst. Chem. Eng.*, 56(6), 1398–1405.

Fleury, M., et al. (2010). "Evaluating sealing efficiency of caprocks for CO storge: An overview of the geocarbone-integrity program and results." *Oil Gas Sci. Technol.*, 65(3), 435–444.

Fox, J. E., Lambert, P. W., Mast, R. F., Nuss, N. W., and Rein, R. D. (1975). "Porosity variation in the Tensleep and its equivalent Weber Sandstone, western Wyoming: A log and petrographic analysis." *Rocky Mountain Association of Geologists Symp.*, Rocky Mountain Association of Geologists, Denver, 185–215.

Frost, C. (2011). "Final report: Carbon sequestration monitoring activities; Dept. of Energy agreement no. DE-NT0004730." *Technical Rep.*, Univ. of Wyoming, Laramie, WY.

Han, W. S., and McPherson, B. J. (2009). "Optimizing geologic CO_2 sequestration by injection in deep saline formations below oil reservoirs." *Energy Convers. Manage.*, 50(10), 2570–2582.

Hansen, A. D. (2007). "Reservoir characterization and outcrop analogs to the Navajo Sandstone in the central Utah Thrust Belt exploration play." M.S. thesis, Dept. of Geology, Brigham Young Univ., Provo, UT.

Harstad, H., Teufel, L., Lorenz, J., and Brown, S. (1996). "Characterization and fluid flow simulation of naturally fratured frontier sandstone, Green River Basin, Wyoming." *Technical Rep. 96-1955, UC-132*, Sandia National Lab, Albuquerque, NM.

Hesse, M. A., Orr, F. M., Jr., and Tchelepi, H. A. (2008). "Gravity currents with residual trapping." *J. Fluid Mech.*, 611(9), 35–60.

Houseknecht, D. W. (1987). "Assessing the relative importance of compaction processes and cementation to reduction of porosity in sandstones." *AAPG Bull.*, 71(6), 633–642.

Huang, N. S., Aho, G. E., Baker, B. H., Matthews, T. R., and Pottorf, R. J. (2011). "Integrated reservoir modeling of a large sour-gas field with

high concentrations of inerts." *SPE Reservoir Eval. Eng.*, 1(8), 418–432.

Ide, S. T., Jessen, K., and Orr, F. M. J. (2007). "Storage of CO_2 in saline aquifers: Effects of gravity, viscous, and capillary forces on amount and timing of trapping." *Int. J. Greenhouse Gas Cont.*, 1(4), 481–491.

Intergovernmental Panel on Climate Change (IPCC). (2005). "Carbon dioxide capture and storage." Chapter 5, *Underground geological storage*, ⟨http://www.ipcc.ch/pdf/special-reports/srccs/⟩ (Dec. 15, 2011).

JMP 9.0 [Computer software]. Cary, NC, SAS Institute.

Konstantinovskaya, E., Rutqvist, J., and Malo, M. (2014). "CO storage and potential fault instability in the St. Lawrence lowlands sedimentary basin (Quebec, Canada): Insights from coupled reservoir-geomechanical modeling." *Int. J. Greenhouse Gas Control*, 22(3), 88–110.

Kumar, A., Noh, M., Pope, G. A., Sepehrnoori, K., Bryant, S., and Lake, L. W. (2004). "Reservoir simualtion of CO_2 storage in deep saline aquifers." *SPE 89343: 2004 SPE/DOE Fourteenth Symp. on Improved Oil Recovery*, Society of Petroleum Engineers, Richardson, TX.

Laubach, S. E. (2003). "Practical approaches to identifying sealed and open fractures." *AAPG Bull.*, 87(4), 561–579.

Laubach, S. E., Reed, R. M., and Lander, R. H. (2010). "Photograph of the month: Fracture with crack-seal texture and porosity, depth 6274 m, Wyoming." *J. Struct. Geol.*, 32(12), 1865.

Lewis, H., and Couples, G. D. (1993). "Production evidence for geological heterogeneities in the Anschutz Ranch East Field, western USA." *Characterization of fluvial and Aeolian reservoirs*, C. P. North and D. J. Prosser, eds., Geological Society of London, Bath, U.K., 321–338.

Li, S. Q., and Zhang, Y. (2014). "Model complexity in carbon sequestration: A design of experiment and response surface uncertainty analysis." *Int. J. Greenhouse Gas Control*, 22(3), 123–138.

Li, S. Q., Zhang, Y., and Zhang, X. (2011a). "A study of conceptual model uncertainty in large scale storage simulation." *Water Resour. Res.*, 47(5), W05534.

Li, S. Q., Zhang, Y., Zhang, X., and Du, C. (2011b). "Geologic modeling and fluid-flow simulation of acid gas disposal in western Wyoming." *AAPG Bull.*, 96(4), 635–664.

Lindquist, S. J. (1983). "Nugget formation reservoir characteristics affecting production in the overthrust belt of southwestern Wyoming." *J. Pet. Technol.*, 35(07), 1355–1365.

Lindquist, S. J. (1988). "Practical characterization of eolian reservoirs for development: Nugget Sandstone, Utah-Wyoming thrust belt." *Sediment. Geol.*, 56(1–4), 315–339.

Liu, B., and Zhang, Y. (2011). "CO_2 modeling in a deep saline aquifer: A predictive uncertainty analysis using design of experiment." *Environ. Sci. Technol.*, 45(8), 3504–3510.

Liu, B., Zhang, Y., and Zhang, X. (2011). "Acid-gas storage in a deep saline aquifer: Numerical sensitivity study to evaluate parameter and model uncertainty." *J. Hazard. Toxic Radioactive Waste*, 10.1061/(ASCE)HZ.1944-8376.0000061, 234–250.

Lu, C., Han, W. S., McPherson, B. J., and Lichtner, P. C. (2009). "Effects of density and mutual solubility of a -brine system on storage in geological formations: 'Warm' vs. 'cold' formations." *Adv. Water Resour.*, 32(12), 1685–1702.

Ma, Y. Z. (2009). "Propensity and probability in depositional facies analysis and modeling." *Math. Geosci.*, 41(7), 737–760.

Ma, Y. Z., Seto, A., and Gomez, E. (2009). "Depositional facies analysis and modeling of the Judy Creek reef complex of the Upper Devonian Swan Hills, Alberta, Canada." *AAPG Bull.*, 93(9), 1235.

Macminn, C. W., Szulczewski, M. L., and Juanes, R. (2010). "CO_2 migration in saline aquifers. Part 1. Capillary trapping under slope and groundwater flow." *J. Fluid Mech.*, 662(11), 329–351.

Michael, K., Golab, A., Shulakova, V., King, J. E., Allinson, G., Sharma, S., and Aiken, T. (2010). "Geological storage of in saline aquifers: A review of the experience from existing storage operations." *Int. J. Greenhouse Gas Control*, 4(4), 659–667.

Milliken, W. J., Levy, M., Strebelle, S., and Zhang, Y. (2007). "The effect of geologic parameters and uncertainties on subsurface flow: Deepwater depositional systems." *SPE 109950: 2007 SPE Annual Technical Conf. and Exhibition*, Society of Petroleum Engineers, Richardson, TX.

Montgomery, D. C. (2008). *Design and analysis of experiments*, 7th Ed., Wiley, Hoboken, NJ.

Morad, S., Al-Ramadan, K., Ketzer, J. M., and De Ros, L. F. (2010). "The impact of diagenesis on the heterogeneity of sandstone reservoirs: A review of the role of depositional facies and sequence stratigraphy." *AAPG Bull.*, 94(8), 1267–1309.

Mosthaf, K. (2007). "CO_2 storage into dipped saline aquifers including ambient water flow." Ph.D. thesis, Univ. of Stuttgart, Stuttgart, Germany.

Myers, R., and Montgomery, D. (1995). *Response surface methodology—Process and product optimization using designed experiments*, Wiley, New York.

Nelson, P. H. (1994). "Permeability-porosity relationships in sedimentary rocks." *Log Analyst*, 35(3), 38–62.

Nordbotten, J., Celia, M. A., Bachu, S., and Dahle, H. K. (2005). "Semi-analytical solution for leakage through an abandoned well." *Environ. Sci. Technol.*, 39(2), 602–611.

Peng, C. Y., and Gupta, R. (2004). "Experimental design and analysis methods in multiple deterministic modeling for quantifying hydrocarbon in-place probability distribution curve." *SPE Asia Pacific Conf. on Integrated Modelling for Asset Management*, Society of Petroleum Engineers, Richardson, TX.

Royse, F. (1993). "An overview of the geological structure of the Thrust Belt in Wyoming, northern Utah and eastern Idaho." *Geol. Surv. Wyoming Memoir*, 5, 273–311.

Schlumberger. (2009a). *ECLIPSE technical manual: The GASWAT option*, Houston, TX.

Schlumberger. (2009b). *Petrel user's manual*, Houston, TX.

Sifuentes, W., Blunt, M. J., and Giddins, M. A. (2009). "Modeling CO_2 storage in aquifers: Assesssing the key contributors to uncertianty." *SPE 123582: 2009 SPE Offshore Europe Oil and Gas Conf. and Exhibition*, Society of Petroleum Engineers, Richardson, TX.

Stauffer, P., Viswanathan, H., Pawar, R., and Guthrie, G. (2009). "A system model for geologic sequestration of carbon dioxide." *Environ. Sci. Technol.*, 43(3), 565–570.

Tillman, L. E. (1989). "Sedimentaty facies and reservoir characteristics of the nugget sandstone (Jurassic), Painter reservoir filed, Uinta County, Wyoming." *Rocky Mountain Association of Geologists Symp.—Sandstone Reservoirs*, Rocky Mountain Association of Geologists, Denver, 97–108.

Yang, G. (2012). "Uncertainty analysis of carbon sequestration in an inclined deep saline aquifer of the Wyoming Overthrust Belt." M.S. thesis, Dept. of Geology and Geophysics, Univ. of Wyoming, Laramie, WY.

Yeten, B., Castellini, A., Guyaguler, B., and Chen, W. H. (2005). "A comparison study on experimental design and response surface methodologies." *SPE 93347: 2005 SPE Reservoir Simulation Symp.*, Society of Petroleum Engineers, Richardson, TX.